Kent Academic Repository

Full text document (pdf)

1   **METHODS PAPER**

2   *Cartesian coordinates in two-dimensional bone histology images ~~are useful~~ in Quaternary bone*

3   *remodelling research*

4   Justyna J. Miszkiewicz[1,2,3], Julien Louys[4], Patrick Mahoney[3]

5   [1]School of Archaeology and Anthropology, Australian National University, Canberra, Australia

6   [2]School of Social Science, University of Queensland, Brisbane, Australia

7   [3]Skeletal Biology Research Centre, University of Kent, Canterbury, United Kingdom

8   [4]Australian Research Centre for Human Evolution, Griffith University, Brisbane, Australia

9

10   **ABSTRACT**

11   Palaeohistologists who work with well-preserved hominin cortical bone can examine two-dimensional

12   (2D) histology images for quantitative parameters of secondary osteons and Haversian canals to

13   reconstruct past bone remodelling. Standard techniques in this space ~~have~~ included ~~taking~~ area

14   measurements and counts of histology components recorded from an ~~seen in an~~ image. The 'point-

15   count' technique involves counting all the items (e.g., secondary osteons, osteocyte lacunae) of interest

16   per image area. The open access image analysis software ImageJ/ FIJI facilitates this technique in a

17   user-friendly way. Raw data points are captured and can be saved in a spreadsheet. Aside from the total

18   number of counts, the software also issues Cartesian (XY) coordinates locating each counted point.

19   These XY coordinates are typically neglected within palaeohistological approaches due their assumed

20   irrelevance to research questions of bone remodelling significance. We provide a short evaluation of

21   XY coordinates captured by ImageJ/FIJI from 2D bone histology images, and a protocol for a simple

22   calculation of XY distances that follow the path of point counting. We focus on osteocyte lacunae which

23   serve as a proxy for osteoblast-osteocyte conversion in live bone by replicating the protocol on a bone

24   sample from a Medieval English individual. We discuss the potential of XY coordinates for

25   reconstructing the proximity of ~~efficient representation of how closely situated the counted~~ osteocyte

26   lacunae~~/points are,~~ and related ~~thus indicating localised~~ bone remodelling activity through exchange of

27   nutrients by neighbouring cells. We recommend palaeohistologists report XY coordinate data in their

28   results to ensure better hominin palaeobiology characterisation.

29   **Keywords**: hominins; image analysis; histomorphometry; bone remodelling; ImageJ

30

31

1. INTRODUCTION

Quantitative analysis of histology images (histomorphometry) is a gold standard in various biological disciplines that collect data about tissue cells and other microscopic structures (e.g., Erben & Glösmann 2019; Revell 1983; O'Driscoll et al. 1999; Villa & Lynnerup 2010). Histology can also be applied to bones that derive from palaeontological and archaeological contexts to reconstruct remodelling processes that occur throughout an animal's lifespan and respond to internal and environmental stimuli (e.g., Bromage et al. 2009; Cook et al. 1998; Crowder & Stout 2011; de Buffrénil et al. 2021; Miszkiewicz 2015; Sawada et al. 2004; Stout & Stanley 1991). One useful analytical approach in bone histology examination is quantifying geometric and density properties of secondary/ Haversian bone tissue seen microscopically in thin sections taken in a transverse plane (Stout & Crowder 2012) (Figure 1). The histological appearance of Haversian bone reflects the activity of Bone Multicellular Units (BMUs) which are three-dimensional (3D) cell structures that execute bone remodelling in live bone by 'digging' longitudinal tunnels as bone is resorbed and deposited (Figure 2) (Lassen et al. 2017; Maggiano et al. 2016; Sims & Martin 2014). Once quantified, cortical bone histology data can be studied at an individual or large sample level representing past populations (e.g., Chan, Crowder & Rogers 2007; Stout & Lueck 1995; Miszkiewicz et al. 2020).
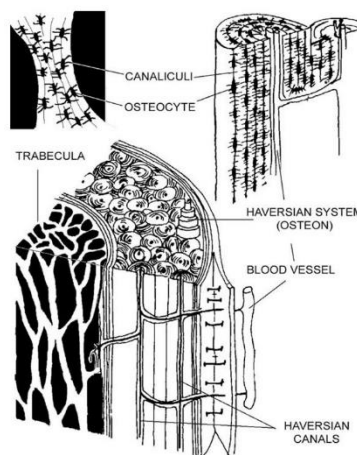
Figure 1. Sketch of the microscopic components of bone showing Haversian systems and osteocytes. Reproduced from Smit et al. 2002 p. 2022, with permissions from John Wiley and Sons under licence 5297961008734.
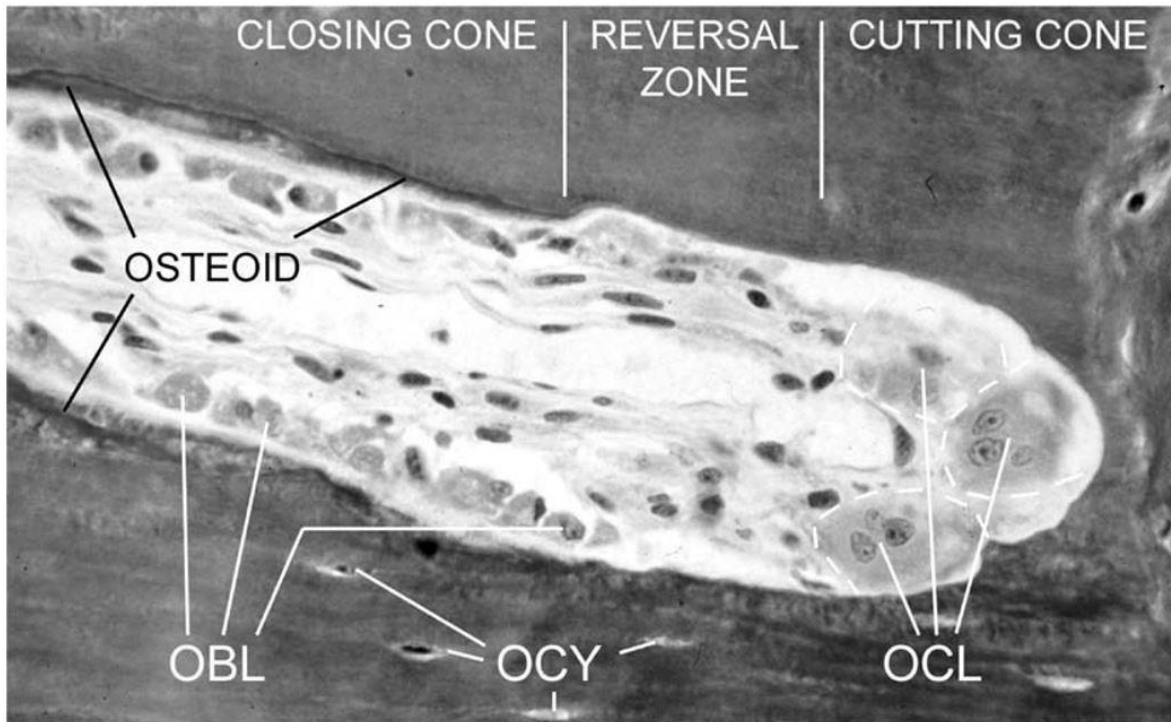
Figure 2. An example of an active Bone Multicellular Unit (BMU) showing osteoclasts (OCL), osteoblasts (OBL), and osteocytes (OCY). Image is not to scale, but the width of the BMU would be approximately 200 μm. Reproduced from Smit et al. 2002 p. 2024, with permissions from John Wiley and Sons under licence 5297961008734.

All bone biologists who undertake histomorphometry are expected to follow recommended guidelines for unified nomenclature and techniques used in calculating parameters of bone remodelling (Dempster et al. 2013). Working with Haversian tissue, the relevant quantifiable histology variables include the area, diameter, density, and circumference of structures such as secondary osteons, Haversian canals, and osteocyte(s)/lacunae (osteocytes do not always preserve in post-mortem bone, so osteocyte lacunae indicate where the osteocytes had resided) (Crowder & Stout 2012; Hunter & Agnew 2016; Stout, Cole & Agnew, 2019; Bromage et al. 2009). The densities of secondary osteons or osteocyte lacunae are typically calculated by summing up the total counts seen in a specified field of view or a selected region of interest (ROI), and then dividing the raw count by the area examined (Crowder & Stout 2012; Crowder et al. 2022; Drew, Mahoney & Miszkiewicz 2021). This counting approach is known as the 'point count' technique (Stout & Stanley 1991). Secondary osteon density, referred to as osteon population density (OPD), data reflect the amount of remodelled bone per area (Frost 1987), whereas osteocyte density reflects osteoblast-osteocyte conversion (Bromage et al. 2016).

73 While these densities have been reported by multiple studies investigating topics that have ranged from

74 biomechanics (Drew, Mahoney & Miszkiewicz, 2021), diet (Paine & Brenton 2006), to human

75 evolution (Sawada et al. 2004), a notable gap in analyses is that the proximities of individual counted

76 points are not considered. This is interesting because biologists regularly consider dispersal or proximity

77 analysis when analysing points against a specified area to assess the randomness, clustering, or

78 migration of cells (Cruz et al. 2005; Fernández, Lysakowski & Goldberg, 1995; Gorelik & Gautreau

79 2014; Wang et al. 2021). Only a handful of palaeontological, bioarchaeology, or anthropological studies

80 haves considered spatial distribution relationships within bone histology sections. This has included

81 Rose et al. (2012), and Gocha and Agnew (2016), who brought to light the value of applying Geographic

82 Information Systems (GIS) software in understanding osteon population dispersal across complete

83 human metatarsal and femoral bone cross-section shafts, respectively. Further, Miszkiewicz et al. (2020)

84 applied GIS to measure distances between neighbouring Haversian canals across thin sections from the

85 femoral midshaft in an archaeological specimen, spatially mapping cortical bone porosity. GIS can

86 require substantial training. An alternative, commonly used, user friendly, and self-intuitive, image

87 analysis software is the open access ImageJ, part of the FIJI package (Schindelin et al. 2015). In this

88 paper, we highlight that ImageJ/FIJI also registers XY coordinates alongside point counts and can be

89 used to efficiently calculate path distances between neighbouring histology structures. We focus on

90 hypothetical osteocyte lacunae in a sketched diagram, supply a manual protocol based on established

91 mathematics for the path distance calculations, and then replicate it on a secondary osteon image from

92 an archaeological (dated to Medieval England) human femur.

93 **2. METHODS: XY COORDINATES IN IMAGEJ/FIJI**

94 **2.1. The protocol and application to a hypothetical sample**

95 ImageJ/FIJI can be freely downloaded from the dedicated website (https://imagej.net/software/fiji/).

96 The preparation of bone histology slides will not be covered here. A ready image with a known scale

97 captured using a dedicated microscope camera is needed to apply the protocol we discuss. We note

98 ImageJ/FIJI provides macros and plug-ins that calculate various other aspects of XY coordinates (e.g.,

99 distance from centroid), but these require coding and script amendments. Distances between selected

100   points can also be measured manually one by one using the "Straight line" tool of ImageJ/FIJI, but this

101   approach takes more time than the presented XY coordinate analysis and has to be conducted in addition

102   to point counting. We provide a manual guide for path distance calculations from the XY coordinate

103   data recorded at the same time as point counts which is straightforward and efficient in its application.

104   The first step (Figure 3a) is to open ImageJ/FIJI (we used vol. 153o), import the image of interest, and

105   set the appropriate scale ("Analyze" > "Set scale"). The counts of the osteocyte lacunae can be

106   completed using the "Multi-point" function selected form the ImageJ/FIJI toolbar. For the distances to

107   be most meaningful biologically, the sequence of counts made would ideally be either conducted

108   starting at the Haversian canal and continuing outwards (towards the cement line), or *vice versa* (Figure

109   3b). That is because canaliculi, which connect successive osteocytes within a secondary osteon, are

110   largely arranged radially so as to maximise fluid flow (van Tol et al. 2020). By pressing "M", the

111   measurements can be obtained. A "Results" window will appear where the following measurements are

112   recorded: "Area", "Mean", "Min", "Max", "X", "Y" (Figure 3c). The "X" and "Y" are the coordinate

113   values that can be used to understand the proximity of these points. The output from the "Results"

114   window can be saved as an Excel spreadsheet, or the XY coordinates can be copied and pasted into a

115   new spreadsheet.
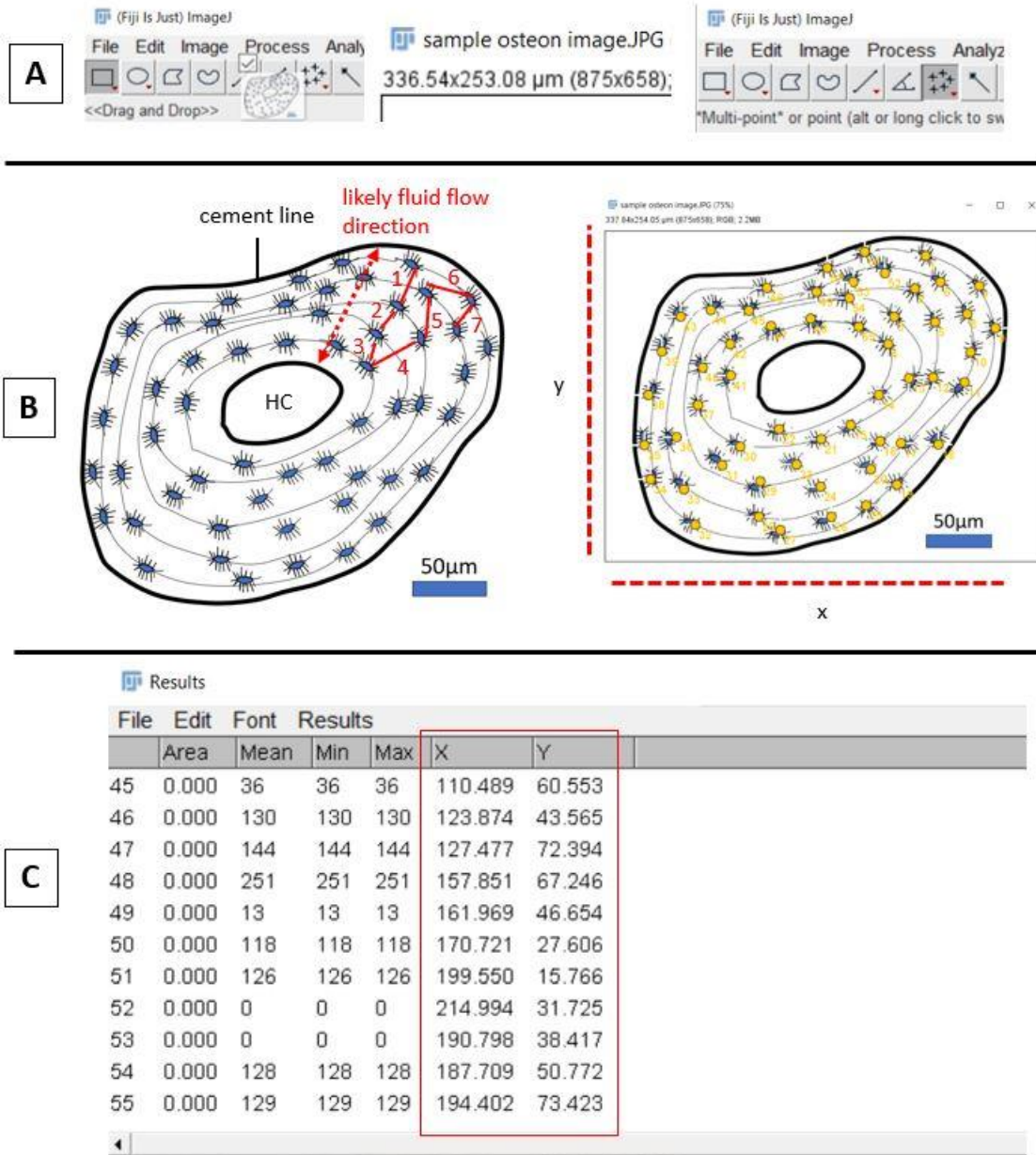
Figure 3. Series of initial steps of point counting in ImageJ/FIJI. A: importing of image (HC: Haversian canal), setting the scale, and selecting the "Multi-Point tool". B: outline of secondary osteon diagram with osteocyte lacunae prior to (left), and after (right), counting of the lacunae. C: ImageJ/FIJI data window showing XY coordinates for each point (red box, left), transported into a spreadsheet (right).

The next step is to calculate the 2D distance between XY coordinates, following the path of counting,

using the formula

$$D = \sqrt{(x_2 - x_1)^2 + (y_2 - y_1)^2}$$

(derived from the Pythagorean theorem) (Figure 4).

1. In the same or a new spreadsheet, new columns aligned next to each other can be created and named: X_{diff} (this will be the difference between successive X coordinates), Y_{diff} (this will be the difference between successive Y coordinates), D^2 (squared distance between X_{diff} and Y_{diff}), D (square root of D^2).

2. The difference between successive X and successive Y coordinates is then calculated individually (i.e., per axis). This can be achieved in Microsoft Excel by typing in "=cell with raw X value-preceding cell with raw X value" - the example in Figure 4 would be "=A3-A2". This then can be repeated on the Y coordinates. The last cell should not be considered because it does not have a successive coordinate. The cell function can be dragged down the entire column.

3. D^2, defined through the formula: $D^2 = X_{diff}^2 + Y_{diff}^2$, is then calculated. This can be achieved in Excel by typing "=cell with X_{diff}^2+cell with Y_{iff}^2". The example shown in Figure 4 would be "=C2^2+D2^2". The cell function can be dragged down the entire column.

4. Finally, the square root of D^2 is calculated which can be done in Excel by typing "=SQRT(cell with D^2 value). In Figure 4, the example would be "=SQRT(E2)". The cell function can be dragged down the entire column.

Raw data resulting from this hypothetical image analysis can be found in our Supplemental File. The resulting D values are the distances in the unit appropriate to the image between the XY coordinates registered along the pathway of counting. They can be analysed across a whole osteon, summarised as averages per osteon, a full image, individual, larger sample – whatever the desired level of analysis as per one's research question. In the presented example, the average distance across this one hypothetical secondary osteon was 28.25 μm (see Supplemental File).
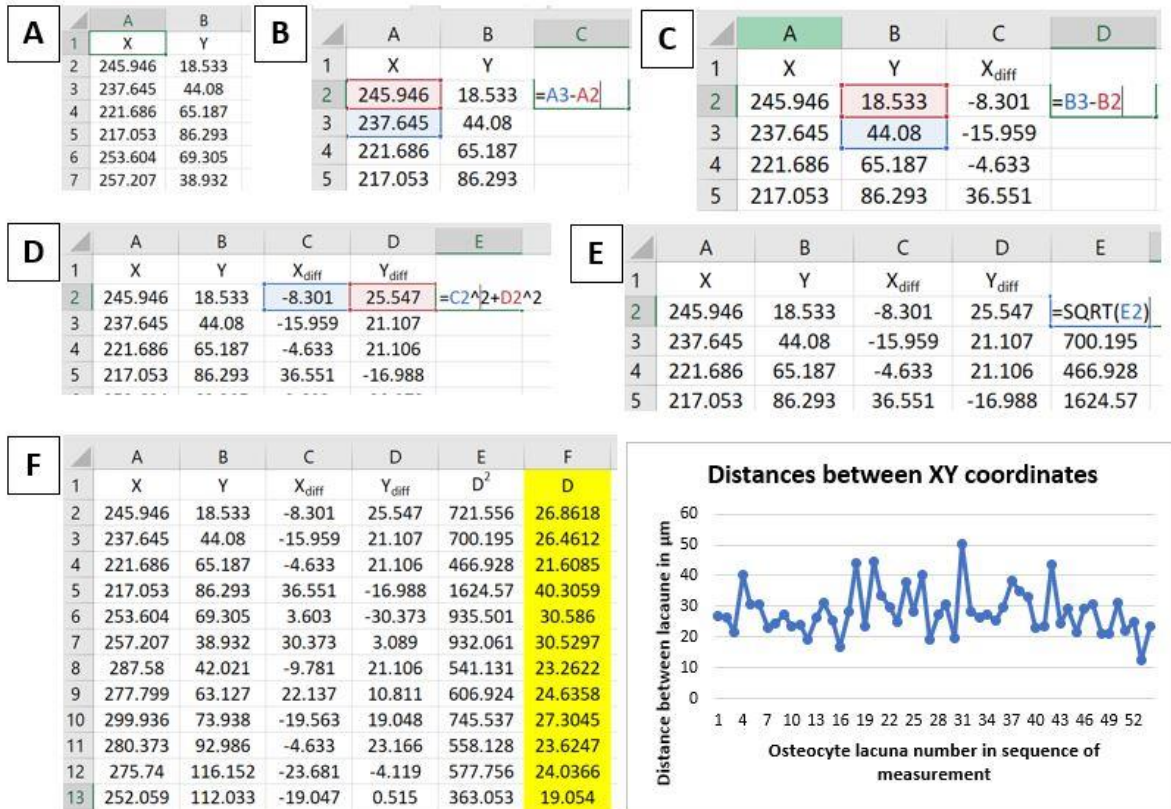
Figure 4. Screenshots of successive steps in XY distance coordinate calculations in Microsoft Excel. A: XY coordinates from the ImageJ/FIJI results output, B-C: calculating differences between successive X and Y coordinates, D: calculating the squared distance (D^2) between XY differences, E: calculating the square root of D^2, F: final distance values of XY coordinates (D) in μm (highlighted in yellow), which can be quickly visualised using a simple line graph.

2.2. Replication on an authentic sample

To validate this short protocol, we applied it step-by-step to a real case – using a cortical bone histology image showing a well-preserved secondary osteon in the femur of a Medieval English individual (ID: NGB89SK2). The thin section is a 100-μm thick slice of midshaft cortex extracted from the anterior aspect of the femur. This individual was estimated to be a middle-aged (35-50 years old) male (Miszkiewicz, 2014), and the sample is part of a larger collection of thin sections representing a Medieval English human osteological assemblage curated at the University of Kent, UK. These thin sections had been prepared following standard histology methods applied to archaeological human remains (Miszkiewicz, 2014). A full ethics board review was not required as this is an archaeological collection, but a local (School of Anthropology and Conservation) ethics application form and check list was filed on 11 November 2010 and approved by the 2010 Ethics Advisory Group at the University

167   of Kent, UK. In addition to curatorial permissions, all analyses on these sections follow codes of ethics

168   and good practice as stipulated by the international biological anthropology bodies (British Association

169   for Biological Anthropology and Osteoarchaeology; American Association of Biological

170   Anthropologists). The anterior femur sample presented here was also previously included in research

171   by Drew, Mahoney and Miszkiewicz et al. (2021), Miszkiewicz and Mahoney (2012), and Miszkiewicz

172   (2014). The XY coordinate distance data are calculated here for the first time.

173   Using an Olympus BX60 high powered microscope equipped with a MIchrome 5 Pro SS-936 camera

174   and operated using Capture v2.1 software, one secondary osteon showing clear cement lines (Figure

175   5A) and well-preserved osteocyte lacunae (Figure 5B) was selected from intra-cortical bone. It was

176   viewed under linearly polarised light to check good preservation, i.e., ensuring that individual

177   concentric lamellar rings could be seen clearly (Figure 5CD).
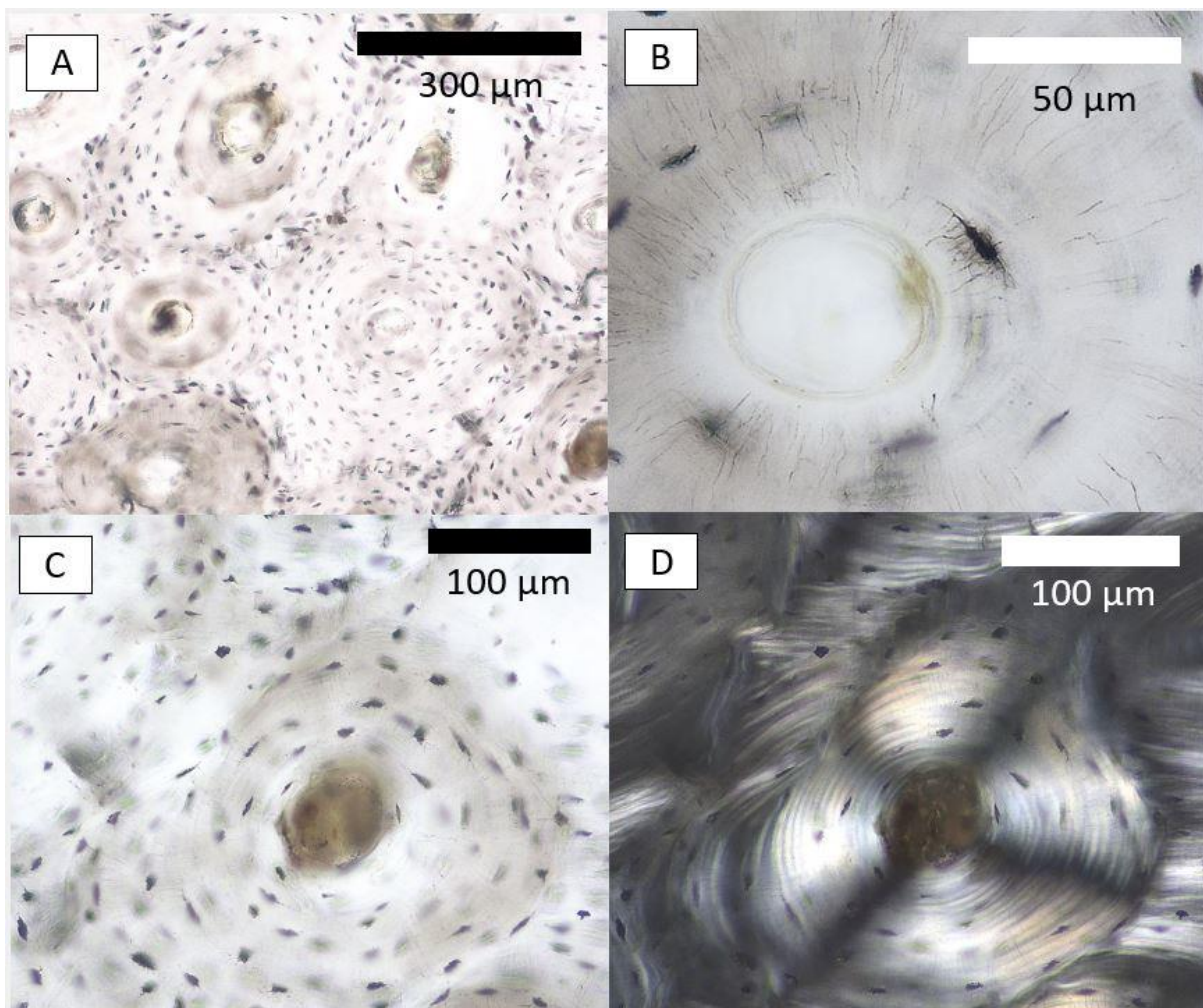
178

179 **Figure 5**. Cortical bone histology images in a sample from a Medieval English male (ID: NGB89SK2,
180 St. Gregory's Priory and Cemetery collection, University of Kent, UK) taken from the anterior midshaft.
181 Image A shows a cluster of secondary osteons with a range of osteocyte lacunae preservation. Image B
182 shows a closeup of an osteocyte lacuna as an example of good preservation in the secondary osteon
183 selected for our replication analysis. Images C and D show the secondary osteon under polarised
184 transmitted (C) and linearly polarised light (D).

185 The secondary osteon image captured using transmitted light (so that each osteocyte lacuna could be

186 identified easily (black lacunae against white bone)) was examined following our protocol above. The

187 image was imported into ImageJ/FIJI (vol. 153o). Osteocyte lacunae were counted starting at the cement

188 line and continuing towards the Haversian canal in a linear fashion (Figure 6). The resulting XY

189 coordinates were used for calculating distances between the neighbouring osteocyte lacuna, the average

190 of which for the entire secondary osteon was 24.84 μm.
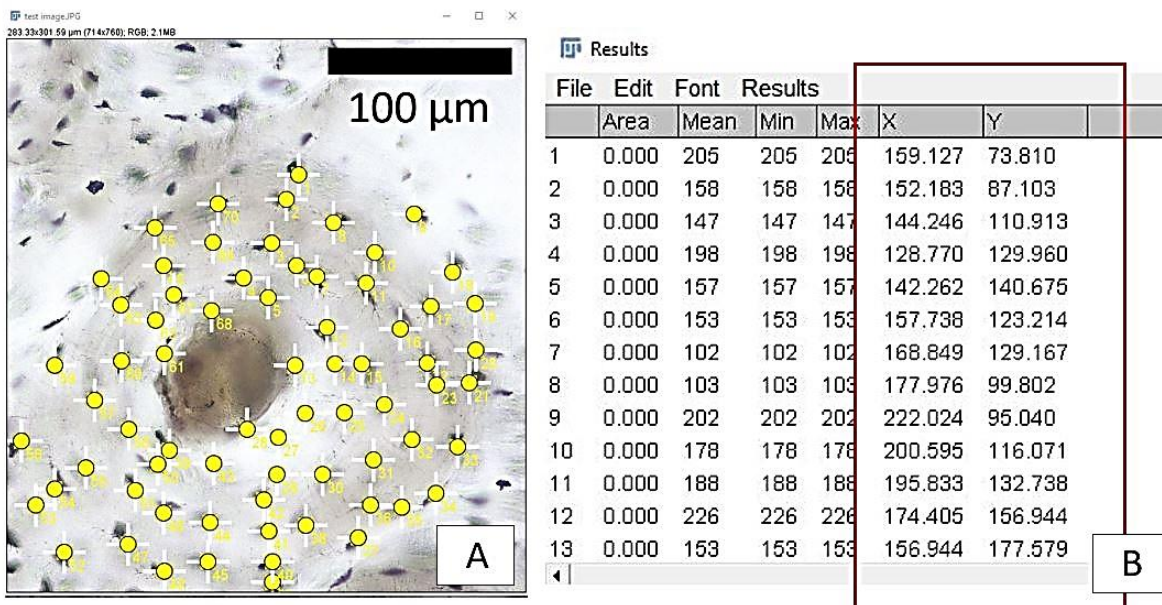
191

192 **Figure 6**. Screenshots of image analysis steps replicating our XY coordinate calculation protocol. A:
193 secondary osteon with osteocyte lacunae (yellow dots). B: raw data output window in ImageJ/FIJI
194 showing resulting XY coordinates (red rectangle).
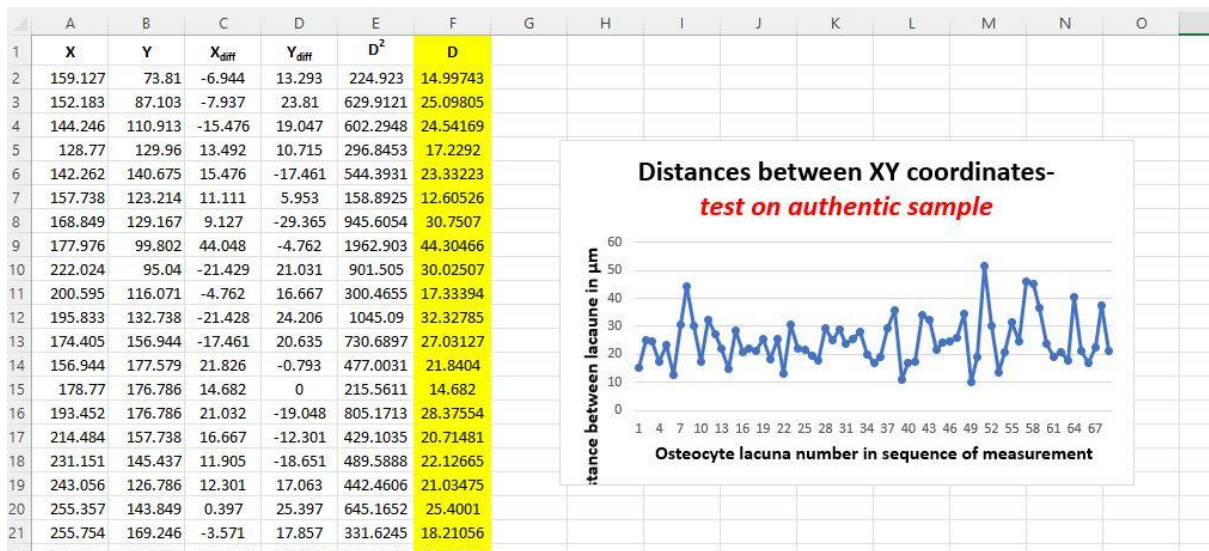
Figure 7. Screenshot of final calculations of distances between XY coordinates yielded using the Medieval English histology sample. Column F, highlighted in yellow, shows the D values in μm. The line graph illustrates variation in D values from across the entire secondary osteon.

3. DISUSSION: INTERPRETATIVE VALUE

We present here a simple and effective way to obtain an insight into the distances between neighbouring points ~~along a path of counting~~ in a 2D histology image. Those who regularly work with osteocyte lacunae or OPD data might already have raw data files from ImageJ/FIJI stored where the XY coordinates are saved. Certainly, whenever possible these should be provided alongside other commonly reported variables, either in the main body of an article or the online supplementary information. Re-analyses of data as outlined here may provide new insights into new or old research questions, although it is also vital to provide the sequence in which the points are counted. For example, very wide distances between some coordinates may simply reflect random and widespread counting across an image and thus have no meaning for understanding distances between neighbouring bone histology elements.

The interpretative value of the distances between osteocyte lacunae on a path of counting is that it would inform how well inter-connected osteocytes were in a given sample. This provides information about bone remodelling processes and how actively bone was maintained (Andreaus, Colloca & Iacoviello 2014; Bromage et al. 2009). This is because the inter-connectedness of neighbouring lacunae facilitates

healthy exchange of nutrients, bone biological signals, and fluid flow (Kollmannsberger et al. 2017; van Tol et al. 2020). For example, it has been suggested that, in humans, osteocyte-to-osteocyte distance of 20-30 μm is enough to facilitate effective dissemination of molecules (Chen et al. 2018; Wang et al. Sugawara et al. 2005). In our Medieval example, the resulting D values fell into this distance range, which could be used to infer that osteocyte communication was not disrupted in this region of bone. Canè et al. (2000) noted changes in osteocyte distribution depending on the long bone region (e.g., cortical vs trabecular bone, diaphysis vs metaphysis vs epiphysis). Thus, future research into osteocyte lacunae distance data applied across hominin bone could be placed within the wider bone biology knowledge and help further refine interpretations made from bone histology density and other geometric variables alone.

The XY coordinate distance measurements may not be as useful in understanding secondary osteon distribution as they might be when applied to osteocyte lacunae, simply because osteons can remodel both stochastically and in a targeted fashion (Martin 2007), so it is almost impossible to determine the timing (sequence of secondary osteon appearance) of remodelling from post-mortem, archaeological, or fossilised bone samples. Identifying the timing of remodelling would also be difficult to achieve when dealing with bone from older individuals that show several generations of remodelled secondary osteons, possibly reflecting an OPD asymptote (Frost 1987). However, the technique could be applicable to counts of intact osteons (see Crowder et al. 2022) across a relatively larger image area (or a shaft cross-section) to determine whether BMU products were operating in a clustered or dispersed manner, alongside the osteon density data.

The key limitation of using the XY coordinate distance in bone histology examination is, of course, the 2D level of perspective which does not capture the 3D nature of osteocytes or osteonal structures in a bone sample (Andronowski & Cole 2021). Another limitation is that the outlined calculations need to be processed manually, in the sense that they have to be analysed outside of ImageJ/FIJI. However, once the main cell functions are set up, the XY coordinates from the ImageJ/FIJI output can be simply copied and pasted into a spreadsheet (a template is supplied in our Supplemental File). The advantage of using ImageJ/FIJI lies in having access to a forum of supporting scholars who are continually

242 developing macros and plug-ins, and assist with coding, that can be used to calculate other XY

243 coordinate distances that might be of interest to palaeohistologists (e.g. distance from centroid). Our

244 protocol does not require significant training or access to expensive software and so would be applicable

245 across a wide range of institutions, particularly where there is limited infrastructure (see Miszkiewicz

246 2020). While other disciplines can employ automated approaches to cell counting and measuring from

247 2D or 3D images (e.g., O'Driscoll et al. 1999), histologists working with archaeological or fossilised

248 samples are hindered by issues with preservation, meaning that careful manual approaches to histology

249 image analysis will continue to be needed. Being able to conduct manual XY coordinate counts could

250 be a useful addition to the technical toolkit.

251 **Acknowledgements**

253 **Competing interests**

254 We have no competing interests to declare.

255 **REFERENCES**

256 Andreaus, U., Colloca, M., & Iacoviello, D. (2014). Optimal bone density distributions: numerical

257 analysis of the osteocyte spatial influence in bone remodeling. *Computer Methods and Programs in*

258 *Biomedicine*, 113(1), 80-91. https://doi.org/10.1016/j.cmpb.2013.09.002

259 Andronowski, J. M., & Cole, M. E. (2021). Current and emerging histomorphometric and imaging

260 techniques for assessing age-at-death and cortical bone quality. *Forensic Science*, 3(2), e1399.

261 https://doi.org/10.1002/wfs2.1399

262 Bromage, T.G., Lacruz, R.S., Hogg, R., Goldman, H.M., McFarlin, S.C., Warshaw, J., Dirks, W.,

263 Perez-Ochoa, A., Smolyar, I., Enlow, D.H., & Boyde, A. (2009). Lamellar bone is an incremental

264 tissue reconciling enamel rhythms, body size, and organismal life history. *Calcified Tissue*

265 *International*, 84(5), 388-404. https://doi.org/10.1007/s00223-009-9221-2

266 Bromage, T.G., Juwayeyi, Y.M., Katris, J.A., Gomez, S., Ovsiy, O., Goldstein, J., Janal, M.N., Hu,

267 B., & Schrenk, F. *2016). The scaling of human osteocyte lacuna density with body size and

268 metabolism. *Comptes Rendus Palevol*, 15(1), 32-39. https://doi.org/10.1016/j.crpv.2015.09.001

269 Canè, V., Marotti, G., Volpi, G., Zaffe, D., Palazzini, S., Remaggi, F., & Muglia, M. A. (1982). Size

270 and density of osteocyte lacunae in different regions of long bones. *Calcified Tissue International*,

271 34(1), 558-563. https://doi.org/10.1007/BF02411304

272 Chan, A. H., Crowder, C. M., & Rogers, T. L. (2007). Variation in cortical bone histology within the

273 human femur and its impact on estimating age at death. *American Journal of Physical Anthropology*,

274 132(1), 80-88. https://doi.org/10.1002/ajpa.20465

275 Chen, X., Wang, L., Zhao, K., & Wang, H. (2018). Osteocytogenesis: roles of physicochemical

276 factors, collagen cleavage, and exogenous molecules. *Tissue Engineering Part B: Reviews*, 24(3),

277 215-225. https://doi.org/10.1089/ten.teb.2017.0378

278 Cook, M., Molto, E. L., & Anderson, C. (1988). Possible case of hyperparathyroidism in a Roman

279 period skeleton from the Dakhleh Oasis, Egypt, diagnosed using bone histomorphometry. *American

280 Journal of Physical Anthropology*, 75(1), 23-30. https://doi.org/10.1002/ajpa.1330750104

281 Crowder, C., & Stout, S. (Eds.). (2011). *Bone Histology: An Anthropological Perspective*. Boca

282 Raton: CRC Press.

283 Crowder, C., Dominguez, V. M., Heinrich, J., Pinto, D., & Mavroudas, S. (2022). Analysis of

284 histomorphometric variables: Proposal and validation of osteon definitions. *Journal of Forensic

285 Sciences*, 67(1), 80-91. https://doi.org/10.1111/1556-4029.14949

286 Cruz, L., Buldyrev, S. V., Peng, S., Roe, D. L., Urbanc, B., Stanley, H. E., & Rosene, D. L. (2005). A

287 statistically based density map method for identification and quantification of regional differences in

288 microcolumnarity in the monkey brain. *Journal of Neuroscience Methods*, 141(2), 321-332.

289 https://doi.org/10.1016/j.jneumeth.2004.09.005

290 de Buffrénil, V., de Ricqlès, A. J., Zylberberg, L., & Padian, K. (Eds.). (2021). *Vertebrate Skeletal

291 Histology and Paleohistology*. CRC Press.

292 Dempster, D.W., Compston, J.E., Drezner, M.K., Glorieux, F.H., Kanis, J.A., Malluche, H., Meunier,

293 P.J., Ott, S.M., Recker, R.R., & Parfitt, A.M. (2013). Standardized nomenclature, symbols, and units

294 for bone histomorphometry: a 2012 update of the report of the ASBMR Histomorphometry

295 Nomenclature Committee. *Journal of Bone and Mineral Research*, 28(1), 2-17.

296 https://doi.org/.10.1002/jbmr.1805

297 Drew, E. R., Mahoney, P., & Miszkiewicz, J. J. (2021). Osteocyte lacuno-canalicular microstructure

298 across the mid-shaft femur in adult males from medieval England. *International Journal of

299 Osteoarchaeology*, 31(2), 176-187. https://doi.org/10.1002/oa.2937

300 Erben R.G., & Glösmann M. (2019). Histomorphometry in rodents. In A. Idris A. (Ed.) *Bone*

301 *Research Protocols*. *Methods in Molecular Biology*, *vol 1914* (pp. 411-435). New York, NY: Humana

302 Press, https://doi.org/10.1007/978-1-4939-8997-3_24

303 Fernández, C., Lysakowski, A. N. N. A., & Goldberg, J. M. (1995). Hair-cell counts and afferent

304 innervation patterns in the cristae ampullares of the squirrel monkey with a comparison to the

305 chinchilla. *Journal of Neurophysiology*, 73(3), 1253-1269. https://doi.org/10.1152/jn.1995.73.3.1253

306 Frost, H. M. (1987). Secondary osteon population densities: an algorithm for estimating the missing

307 osteons. *American Journal of Physical Anthropology*, 30(S8), 239-254.

308 https://doi.org/10.1002/ajpa.1330300513

309 Gocha, T. P., & Agnew, A. M. (2016). Spatial variation in osteon population density at the human

310 femoral midshaft: histomorphometric adaptations to habitual load environment. *Journal of Anatomy*,

311 228(5), 733-745. https://doi.org/10.1111/joa.12433

312 Gorelik, R., & Gautreau, A. (2014). Quantitative and unbiased analysis of directional persistence in

313 cell migration. *Nature Protocols*, 9(8), 1931-1943. https://doi.org/10.1038/nprot.2014.131

314 Hunter, R. L., & Agnew, A. M. (2016). Intraskeletal variation in human cortical osteocyte lacunar

315 density: implications for bone quality assessment. *Bone Reports*, 5, 252-261.

316 https://doi.org/10.1016/j.bonr.2016.09.002

317 Kollmannsberger, P., Kerschnitzki, M., Repp, F., Wagermaier, W., Weinkamer, R., & Fratzl, P.

318 (2017). The small world of osteocytes: connectomics of the lacuno-canalicular network in bone. *New*

319 *Journal of Physics*, 19(7), 073019. https://doi.org/10.1088/1367-2630/aa764b

320 Lassen, N.E., Andersen, T.L., Pløen, G.G., Søe, K., Hauge, E.M., Harving, S., Eschen, G.E.T. and

321 Delaisse, J.M. (2017). Coupling of bone resorption and formation in real time: new knowledge gained

322 from human Haversian BMUs. *Journal of Bone and Mineral Research*, 32(7), 1395-1405.

323 https://doi.org/10.1002/jbmr.3091

324 Maggiano, I. S., Maggiano, C. M., Clement, J. G., Thomas, C. D. L., Carter, Y., & Cooper, D. M.

325 (2016). Three-dimensional reconstruction of Haversian systems in human cortical bone using

326 synchrotron radiation-based micro-CT: morphology and quantification of branching and transverse

327 connections across age. *Journal of Anatomy*, 228(5), 719-732. https://doi.org/10.1111/joa.12430

328 Martin, R. B. (2007). Targeted bone remodeling involves BMU steering as well as activation. *Bone*,

329 40(6), 1574-1580. https://doi.org/10.1016/j.bone.2007.02.023

330 Miszkiewicz, J. J. (2014). Ancient human bone histology and behaviour. PhD Thesis, University of

331 Kent.

332 Miszkiewicz, J. J. (2015). Histology of a Harris line in a human distal tibia. *Journal of Bone and*

333 *Mineral Metabolism*, 33(4), 462-466. https://doi.org/10.1007/s00774-014-0644-0

334

335 Miszkiewicz, J. (2020). The importance of open access software in the analysis of bone histology in

336 biological anthropology. *Evolutionary Anthropology* 29(4), 165-167

337 https://doi.org/10.1002/evan.21859

338 Miszkiewicz, J. J., & Mahoney, P. (2012). Bone microstructure and behaviour in "gracile" and "robust"

339 adult males from the Medieval Period, Canterbury, UK. *American Journal of Physical Anthropology*,

340 147(54), 215-216.

341 Miszkiewicz, J.J., Rider, C., Kealy, S., Vrahnas, C., Sims, N.A., Vongsvivut, J., Tobin, M.J., Bolunia,

342 M.J.L.A., De Leon, A.S., Peñalosa, A.L. and Pagulayan, P.S., 2020. Asymmetric midshaft femur

343 remodeling in an adult male with left sided hip joint ankylosis, Metal Period Nagsabaran, Philippines.

344 *International Journal of Paleopathology*, 31, 14-22. https://doi.org/10.1016/j.ijpp.2020.07.003

345 O'Driscoll, S. W., Marx, R. G., Fitzsimmons, J. S., & Beaton, D. E. (1999). Method for automated

346 cartilage histomorphometry. *Tissue Engineering*, 5(1), 13-23. https://doi.org/10.1089/ten.1999.5.13

347 Paine, R. R., & Brenton, B. P. (2006). Dietary health does affect histological age assessment: an

348 evaluation of the Stout and Paine (1992) age estimation equation using secondary osteons from the

349 rib. *Journal of Forensic Sciences*, 51(3), 489-492. https://doi.org/10.1111/j.1556-4029.2006.00118.x

350 Revell, P. A. (1983). Histomorphometry of bone. *Journal of Clinical Pathology*, 36(12), 1323-1331.

351 http://dx.doi.org/10.1136/jcp.36.12.1323

352 Rose, D. C., Agnew, A. M., Gocha, T. P., Stout, S. D., & Field, J. S. (2012). The use of geographical

353 information systems software for the spatial analysis of bone microstructure. *American Journal of*

354 *Physical Anthropology*, 148(4), 648-654. https://doi.org/10.1002/ajpa.22099

355 Sawada, J., Kondo, O., Nara, T., Dodo, Y., & Akazawa, T. (2004). Bone histomorphology of the

356 Dederiyeh Neanderthal child. *Anthropological Science*, 112(3), 247-256.

357 https://doi.org/10.1537/ase.00094

358 Schindelin, J., Rueden, C. T., Hiner, M. C., & Eliceiri, K. W. (2015). The ImageJ ecosystem: An open

359 platform for biomedical image analysis. *Molecular Reproduction and Development*, 82(7), 518-529.

360 https://doi.org/10.1002/mrd.22489

361 Sims, N. A., & Martin, T. J. (2014). Coupling the activities of bone formation and resorption: a

362 multitude of signals within the basic multicellular unit. *BoneKEy Reports*, 3.

363 https://doi.org/10.1038/bonekey.2013.215

364 Smit, T. H., Burger, E. H., & Huyghe, J. M. (2002). A case for strain-induced fluid flow as a regulator

365 of BMU-coupling and osteonal alignment. *Journal of Bone and Mineral Research*, 17(11), 2021-

366 2029. https://doi.org/10.1359/jbmr.2002.17.11.2021

367 Stout, S. D., & Stanley, S. C. (1991). Percent osteonal bone versus osteon counts: the variable of

368 choice for estimating age at death. *American Journal of Physical Anthropology*, 86(4), 515-519.

369 https://doi.org/10.1002/ajpa.1330860407

370 Stout, S. D., & Crowder, C. (2012). Bone remodeling, histomorphology, and histomorphometry. In C.

371 Crowder & S. D. Stout (Eds.) *Bone Histology: An Anthropological Perspective* (pp. 1-22). Boca

372 Raton: CRC Press.

373 Stout, S. D., & Lueck, R. (1995). Bone remodeling rates and skeletal maturation in three

374 archaeoloqical skeletal populations. *American Journal of Physical Anthropology*, 98(2), 161-171.

375 https://doi.org/10.1002/ajpa.1330980206

376 Stout, S. D., Cole, M. E., & Agnew, A. M. (2019). Histomorphology: Deciphering the metabolic

377 record. In J. E. Buikstra (Ed.) *Ortner's Identification of Pathological Conditions in Human Skeletal*

378 *Remains* (pp. 91-167). Elsevier Academic Press.

379 Sugawara, Y., Kamioka, H., Honjo, T., Tezuka, K. I., & Takano-Yamamoto, T. (2005). Three-

380 dimensional reconstruction of chick calvarial osteocytes and their cell processes using confocal

381 microscopy. *Bone*, 36(5), 877-883. https://doi.org/10.1016/j.bone.2004.10.008

382 Wang, L., Cowin, S. C., Weinbaum, S., & Fritton, S. P. (2000). Modeling tracer transport in an osteon

383 under cyclic loading. *Annals of Biomedical Engineering*, 28(10), 1200-1209.

384 https://doi.org/10.1114/1.1317531

385 Wang, M., Han, X., Liu, C., Takayama, R., Yasugi, T., Ei, S.I., Nagayama, M., Tanaka, Y. and Sato,

386 M., 2021. Intracellular trafficking of Notch orchestrates temporal dynamics of Notch activity in the

387 fly brain. *Nature Communications*, 12(1), 1-15. https://doi.org/10.1038/s41467-021-22442-3

388 van Tol, A.F., Roschger, A., Repp, F., Chen, J., Roschger, P., Berzlanovich, A., Gruber, G.M., Fratzl,

389 P. and Weinkamer, R., 2020. Network architecture strongly influences the fluid flow pattern through

390 the lacunocanalicular network in human osteons. *Biomechanics and Modeling in Mechanobiology*,

391 19(3), 823-840. https://doi.org/10.1007/s10237-019-01250-1

392 Villa, C., & Lynnerup, N. (2010). A stereological analysis of the cross-sectional variability of the

393 femoral osteon population. *American Journal of Physical Anthropology*, 142(3), 491-496.

394 https://doi.org/10.1002/ajpa.21269